Distribution of Particles in Human Stem Cell-Derived 3D Neuronal Cell Models: Effect of Particle Size, Charge and Density

Ewa Czuba-Wojnilowicz,[§] Sara Miellet,[ǀ] Agata Glab,[§] Serena Viventi,[¶] Francesca Cavalieri,[§] Christina Cortez-Jugo,[§] Mirella Dottori,*[ǀ,¶] and Frank Caruso*[§]*

[§]ARC Centre of Excellence in Convergent Bio-Nano Science and Technology, and the Department of Chemical Engineering, The University of Melbourne, Parkville, Victoria 3010, Australia

[ǀ]Illawarra Health and Medical Research Institute, Molecular Horizons, School of Medicine, University of Wollongong, Wollongong, New South Wales 2522, Australia

[¶]Department of Biomedical Engineering, The University of Melbourne, Parkville, Victoria 3010, Australia

Corresponding authors. E-mail address: christina.cortez@unimelb.edu.au; mdottori@uow.edu.au; fcaruso@unimelb.edu.au

ABSTRACT

Neurodegenerative diseases are generally characterized by a progressive loss of neuronal subpopulations, with no available cure to date. One of the main reasons for the limited clinical outcomes of new drug formulations is the lack of appropriate in vitro human cell models for research and validation. Stem cell technologies provide an opportunity to address this challenge by using patient-derived cells as a platform to test various drug formulations, including particle-based drug carriers. The therapeutic efficacy of drug delivery systems relies on efficient cellular uptake of the carrier and can be dependent on its size, shape, and surface chemistry. Although considerable efforts have been made to understand the effects of the physiochemical properties of particles on two-dimensional cell culture models, little is known of their effect in three-dimensional (3D) cell models of neurodegenerative diseases. Herein, we investigated the role of particle size (235–1000 nm), charge (cationic and anionic), and density (1.05 and 1.8 g cm^{-3}) on the interactions of particles with human embryonic stem cell-derived 3D cell cultures of sensory neurons, called sensory neurospheres (sNSP). Templated layer-by-layer particles, with silica or polystyrene cores, and self-assembled glycogen/DNA polyplexes were used. Particles with sizes of <280 nm effectively penetrated sNSP. Additionally, effective plasmid DNA delivery was observed up to six days post-transfection with glycogen/DNA polyplexes. The findings provide guidance in nanoparticle design for therapies aimed at neurodegenerative diseases, in particular Friedreich's ataxia, whereby sensory neurons are predominantly affected. They also demonstrate the application of 3D models of human sensory neurons in pre-clinical drug development.

KEYWORDS: nanoparticle, layer-by-layer, glycogen, sensory neurons, human embryonic stem cells, Friedreich's ataxia

1. INTRODUCTION

Current advances in nanotechnology present an opportunity to develop therapeutic strategies for targeting diseases that are not effectively treatable with conventional methods.[1] Drug delivery systems based on chemically engineered micro- and nanoparticles can encapsulate therapeutic cargos, such as proteins, nucleic acid, and/or small molecular weight drugs,[2,3] and improve their therapeutic efficacy.[4] Using nanoparticle-based formulations is often advantageous, as it can increase the stability of the drug in biological fluids and inhibit its enzymatic degradation in the bloodstream, improve its transportation through biological membranes, and minimize off-target immune response activation.[5] The use of targeting ligands potentially allows for cell-specific drug delivery with minimal side effects,[6] and the composition and type of particles used determine the mechanism of drug loading. Recent evidence suggests that the physicochemical properties of the carrier, including size, shape, and charge, play an important role in determining particle–cell interactions.[7–9] However, reports on the influence of these properties on cell association, internalization, and toxicity largely focus on two-dimensional (2D) cell culture models, particularly neuronal cell models.[10] Although 2D models are useful in providing information about the in vitro behavior of newly engineered delivery systems, there are diseases in which 2D cell models are too simplistic and lack important characteristics of physiologically relevant in vivo structures, as seen with the development of cancer therapeutics.[11] Previously available 2D models used for pre-clinical drug screening lack features such as the extracellular matrix (ECM), enhanced cell-to-cell contact, hypoxia and necrosis present in the in vivo tumours.[12–14] Therefore, inadequate in vitro models can often lead to the poor clinical outcome of initially promising nanoformulations.[15]

Drug development in the neuroscience field has also suffered from the lack of appropriate in vitro models, hence there is a need for more advanced in vitro cell models for the development of therapies aimed at neurodegenerative diseases.[16] The development of stem cell technologies in recent years introduced new opportunities for nanomedicine by providing more accurate disease models.[17] Cells obtained from patients carry a unique genetic profile of the disease and can be differentiated to any cell type, including neurons, and the possibility to culture them in a three-dimensional (3D) structure allows the establishment of in vitro models that can mimic the structural complexity of the human nervous system.[18,19] More advanced, stem cell-derived 3D cell models mimicking brain architecture have been shown to be superior to 2D models while studying the electrophysiological interaction of cells,[20] cell differentiation[21–23] and cell–ECM interactions.[24] Additionally, when used in combination with cell replacement therapy, differentiated cells could be treated with a drug ex vivo, followed by in vivo transplantation of patient-derived cells, thus minimizing the risk of donor cell rejection.[25]

A disease that lacks an accurate pre-clinical model is Friedreich's ataxia (FRDA), which primarily affects the peripheral nervous system.[26] It is a genetic disease caused by a mutation in the frataxin gene (*FXN*), which results in a reduced level of mitochondrial protein frataxin (FXN) involved in iron metabolism.[27] FRDA manifests in progressive degeneration of sensory neurons in the dorsal root ganglia (DRG).[28] Dottori and co-workers established a protocol to obtain 3D cultures of DRG sensory neurons, called sensory neurospheres (sNSP), derived from human embryonic stem cells (hESC).[28,29] sNSP consist of a heterogeneous population of sensory neurons subtypes and provide a useful platform to study various drug formulation for therapies to treat FRDA and other diseases that affect sensory neurons.

In the present study, we report the influence of the physicochemical properties of particles on their association, penetration, and distribution in sNSP. Previous studies have reported the toxicity of particles in neuronal cell lines,[30–32] and Leite et al. have recently studied the interactions between modified gold and polylactic acid nanoparticles and 3D hESC-derived brain organoids.[32] Herein, versatile layer-by-layer (LbL) particle systems with various sizes (235–1000 nm), surface charges (positive and negative), and densities (silica and polystyrene cores) were used. Additionally, a soft, self-assembled nanoparticle system was examined to deliver *FXN*-expressing plasmid DNA as a therapeutic strategy for FRDA; this nanoparticle system is based on bovine glycogen chemically modified with ethylenediamine, which was previously used to deliver small interfering ribonucleic acid (siRNA) into tumor spheroids.[33] Our results provide useful guidance for designing particles for drug delivery into 3D neurodegenerative disease cell models and for applying such models for investigating therapeutic agents for the treatment of FRDA.

2. EXPERIMENTAL

2.1. Materials

Silica (Si) particles (0.235, 0.387, and 0.837 μm, 5% w/v aqueous solution) and FluoGreen polystyrene (PS) particles (0.288, 0.450, and 1.01 μm, 5% w/v aqueous solution) were purchased from microParticles GmbH (Berlin, Germany). Poly(ethylenimine) (PEI; M_w 10000–25000), 50 wt% solution in water), poly-L-arginine hydrochloride (M_w >70000), poly(sodium 4-styrenesulfonate) (PSS; M_w ~70000), bovine liver glycogen (BG), ethylenediamine (EDA), sodium (meta)periodate, sodium cyanoborohydride, bovine serum albumin (BSA), sodium acetate, sodium bicarbonate, Dulbecco's phosphate buffered saline (DPBS), without calcium chloride or magnesium chloride, Accutase, and agarose were purchased from Sigma-Aldrich (St. Louis, MI, USA). Plasmid DNA (pEGFP, 3 kbp) was obtained from the Commonwealth Scientific and

Industrial Research Organisation (Australia). Optimal cutting temperature (OCT) medium was purchased from ProSciTech (Kirwan, Australia). Sodium chloride (NaCl) was purchased from Chem-Supply (Gillman, Australia). Alexa Fluor 647 *N*-hydroxysuccinimide (NHS) dye, wheat germ agglutinin (WGA), Alexa Fluor 488 conjugate (WGA-AF_{488}), Hoechst 33342 (10 mg mL^{-1} solution in water), N2B27 medium, Dulbecco's modified Eagle's medium (DMEM)/F12 medium, insulin, transferrin, and selenium additives, N2 supplement, retinol-free B27 supplement, penicillin-streptomycin, and GlutaMAX were purchased from Life Technologies (Scoresby, Australia). Dialysis tubing (molecular weight cutoff (MWCO) 3.5 kDa) and Nunc Lab-Tek II Chamber microscopy slides were purchased from Thermo Fisher Scientific (Scoresby, Australia). DNA electrophoresis sample loading dye was purchased from Bio-Rad (Gladesville, Australia). DMEM (with 4.5 g L^{-1} glucose and L-glutamine) and trypsin (10X) were purchased from Lonza (Basel, Switzerland). Fetal bovine serum was purchased from Bovogen Biologicals (Keilor East, Australia). Paraformaldehyde 4% aqueous solution (EM grade) was purchased from Electron Microscopy Sciences. Vitronectin and Tesr-E8 basal medium were purchased from STEMCELL Technologies. Brain-derived neurotrophic factor (BDNF), SB431542, and neutrotrophin-3 (NT-3) were purchased from STEMCELL Technologies. Illustra NAP-5 columns were purchased from GE Healthcare and Life Sciences (Silverwater, Australia). CHIR99021 was purchased from Sigma-Aldrich, bone morphogenetic protein 2 (BMP2) was purchased from In Vitro Technologies. Milli-Q water was obtained from a Millipore Milli-Q purification system (Millipore Corporation, Billerica, MA, USA).

2.2. Particle Preparation

2.2.1. Particles with a Si Core. Si particles with sizes 235, 387, and 837 nm were used to deposit film composed of PEI (prepared as 2 mg mL^{-1} solution in Milli-Q water with 1 M NaCl), PSS

(prepared as 1 mg^{-1} solution in 50 mM sodium acetate buffer pH 5.2 with 0.5 M NaCl), and poly-L-arginine (PLArg; prepared as 1 mg mL^{-1} solution in 50 mM sodium acetate buffer pH 5.2). The Si particles (40 μL, 0.05 wt%) were first washed with water three times by centrifugation/resuspension cycles. The centrifugation speed was varied according to the particle size: 1500 *g* for 3 min for 235 nm and 387 nm Si particles and 500 *g* for 1.5 min for 837 nm Si particles. After each centrifugation step, the supernatant was removed, and the particle pellet was resuspended in 200 μL of Milli-Q water. After the third wash, the pellet was resuspended in 200 μL of Milli-Q water, and 200 μL of PEI was added to the particle suspension. After 15 min of mixing at room temperature (21 °C), excess PEI was removed by four centrifugation/resuspension cycles as described above, using 50 mM sodium acetate buffer, pH 5.2 in the last two washes. The same buffer was used in all subsequent steps during washing and adsorption. After PEI coating, subsequent film formation on the particles involved the deposition of PSS-PLArg bilayer for the positively charged particles (terminated with PLArg) and PSS-PLArg-PSS for the negatively charged particles (terminated with PSS). The final particles were resuspended in 100 μL of sodium acetate buffer and stored at 4 °C until further use. Some particles were collected after the final deposition step for ζ-potential measurements and particle counting.

2.2.2. Particles with a PS Core. FluoGreen PS particles (40 μL, 5% w/v) with sizes 288, 450, and 1000 nm were washed three times with 200 μL of Milli-Q water by centrifugation/resuspension cycles. The centrifugation speed was varied according to the particle size: 10000 *g* for 10 min for 288 nm and 450 nm particles and 1000 *g* for 3 min for 1000 nm particles. Positively charged particles were fabricated by deposition of PEI. Briefly, after the last washing step, the pellet was resuspended in 200 μL of Milli-Q water, and 200 μL of PEI solution (2 mg mL^{-1} in Milli-Q water solution with 1 M NaCl) was added, followed by 15 min of mixing

at room temperature and three washes by centrifugation/resuspension as described above. Uncoated PS particles, i.e. without a PEI layer, were used as negatively charged particles. Uncoated or PEI-coated PS particles were resuspended in 100 µL of Milli-Q water and stored at 4 °C until further use. Some particles were collected after the final deposition step for ζ-potential measurements and particle counting.

2.2.3. Synthesis of BG-EDA. BG nanoparticles functionalized with EDA were synthesized according to a previously described method.[33] Briefly, 100 mg of commercially available BG was dissolved in 6 mL of 0.6 M acetic buffer (pH 5.0), followed by the addition of 0.12 mmol sodium periodate and subsequent incubation for 2 h with stirring in the dark. Then, 0.6 mmol of EDA was added, followed by the prompt addition of 1.2 mmol sodium cyanoborohydride. The reaction was incubated overnight and the product was purified by dialysis against Milli-Q water and freeze-dried.

2.3. Preparation of Fluorescently Labeled Particles

Fluorescently labeled particles with a silica core were prepared using Alexa Fluor 647-labeled PLArg (AF_{647}-PLArg) as the third layer in the LbL film assembly. To prepare AF_{647}-PLArg, 5 mg of PLArg (M_w > 70000) was dissolved in 2.5 mL of 50 mM sodium acetate buffer, pH 5.2. AF_{647}-NHS dye (2.4×10^{-4} mmol) was added to the solution and incubated for 4 h with mixing and in the dark. Unbound dye was removed by dialysis (MWCO 3.5 kDa) in Milli-Q water for 2 days (the water was replaced 5 times). The final product was freeze-dried and stored at 4 °C until further use. Particles with a PS core were purchased as fluorescently labeled FluoGreen-PS particles and no further fluorescent labeling was required.

Fluorescently labeled BG-EDA nanoparticles were prepared by addition of 20 µL of 1 mg mL^{-1} Alexa Fluor 647-NHS dye to 4 mg mL^{-1} BG-EDA (2 mg of BG-EDA in 0.5 mL of 0.1 M sodium

bicarbonate buffer at pH 8). The reaction was carried out for 4 h in the dark at room temperature. Unreacted dye was removed using Illustra NAP-5 filter columns (GE Healthcare) as per manufacturer protocol and freeze-dried.

2.4. Particle Characterization

ζ-Potential measurements were performed by microelectrophoresis using a Zetasizer Nano-ZS instrument (Malvern Instruments). A particle suspension (2 µL) was dispersed in 998 µL of Milli-Q water. All measurements were performed in folded capillary cells (DTS1070, Malvern Instruments) at 25 °C. Particle counting (LbL particles) was performed using an Apogee A50-Microflow cytometer to determine particle concentration. For the analysis, 2 µL of particles was added to 398 µL of MilliQ-water and the forward scatter (FSH) vs side scatter (SSH) plots were used. Imaging of particles in solution was performed using a Nikon A1R confocal microscope.

AFM imaging (in air) of BG-EDA nanoparticles was carried out in AC mode using a Cypher ES atomic force microscope (Asylum Research, USA). The cantilever used was Tap300 from Budget Sensors with a resonance frequency of 300 kHz and a spring constant of 40 N m^{-1}. Before imaging, BG-EDA nanoparticles were deposited on freshly cleaved mica and dried at a concentration of 0.01 mg mL^{-1}.

2.5.Complexation of Plasmid DNA

The formation of the BG-EDA/DNA complex was studied using agarose gel electrophoresis. Model pEGFP plasmid (3 kbp) expressing green fluorescent protein was prepared as a solution in DPBS (0.4 µg mL^{-1}). A 2 mg mL^{-1} BG-EDA solution was prepared in DPBS. Complex formation was studied using varying BG-EDA-to-plasmid DNA mass ratios (0.5, 1, 10, 15, 20, and 30 w/w) in 30 µL final volume and incubated at room temperature for 30 min. Next, 5 µL of nucleic acid loading dye was added and mixed for 10 s by vortexing. Then, 30 µL of solution containing BG-

EDA/DNA complexes was loaded onto 1.6% agarose gel and electrophoresis was performed for 30 min at 150 V. Control samples containing only DNA or BG-EDA were prepared in 30 μL of DPBS.

Aqueous phase AFM imaging of BG-EDA nanoparticles complexed with pDNA (weight ratio of 20) was performed in 0.2× PBS using a Cypher ES atomic force microscope (Asylum Research, USA) with BlueDrive. The cantilever used was BL-AC40-TS from Asylum Research with a spring constant of 0.09 N m^{-1} and a resonance frequency of 30 Hz in liquid. 3D images were processed using Igor 6.37. Prior to imaging, BG-EDA/DNA complexes were placed on freshly cleaved mica and incubated at room temperature for 1 h to allow for the settling of the particles.

2.6. Generation of sNSP

hESC (WA09, WiCell) were maintained as bulk culture in feeder-free conditions on vitronectin-(STEMCELL Technologies) coated dishes using TeSR-E8 basal medium (STEMCELL Technologies). For neural induction to neural crest progenitors, cells were plated on a laminin-coated organ culture dish in TeSR-E8 medium. After 24 h, the medium was removed and replaced with neural basal medium (NBM)-DMEM/F12 medium (1:1 mixture) supplemented with 1% N2 and 1% B-27 supplements, 1% Insulin-Transferrin-Selenium-Sodium Pyruvate (ITS-A), 1% L-glutamine, 0.3% glucose supplemented with CHIR99021 and SB431542 (3 and 10 μM, respectively). Media was changed every 2–3 days. After 5 days of incubation, cells were harvested and plated in U-bottom ultra-low attachment 96-multiwell plates (Corning) in NBM supplemented with 1% N2 and 1% B-27 supplements, 1% IST-A, 1% L-glutamine, and 1% penicillin/streptomycin/amphotericin. This medium was also supplemented with BMP2 and FGF2 (10 and 20 ng mL^{-1}, respectively) to form sNSP. Half media changes (50% of old media replaced with fresh media) were performed every 2–3 days. After 6–8 days of incubation, the medium was

replaced with NBM medium supplemented with 1% N2 and 1% B-27, 1% IST-A, 1% L-glutamine, 1% penicillin/streptomycin/amphotericin as well as 10 μg mL^{-1} of Y27, 10 ng mL^{-1} BDNF, beta nerve growth factor (β-NGF), NT-3, and glial-derived neurotrophic factor (GDNF) for 1 week. sNSP were incubated further for 6–8 days in NBM supplemented with 1% N2 and 1% B-27 supplements, 1% IST-A, 1% L-glutamine and 1% penicillin/streptomycin/amphotericin. In these experiments, sNSP were used after 3 weeks of growth and were typically 300–500 μm in diameter.

2.7. Particle–sNSP Incubation

2.7.1. LbL Si Core Particles and PS Particles. sNSP cultured in 96-well round-bottom plates were placed in 200 μL of fresh NBM culture medium. Particle suspensions (Si 837, 387, and 235 nm, and PS 1000, 450, and 288 nm) were prepared at 3.0×10^7 particles in 30 μL of Milli-Q water. The cell number in one sNSP is estimated to range from 1×10^5 to 3×10^5, which corresponds to a particle-to-cell ratio ranging from 100 to 300, respectively. For the static cell culture, sNSP were incubated with particles for 72 h at 37 °C, 5% CO_2 in a humidified atmosphere. For the dynamic cell culture incubation, plates were mounted onto orbital shaking platforms set at 120 rpm and incubated for 72 h at 37 °C, 5% CO_2 in a humidified atmosphere.

2.7.2. Amine-Modified BG Particles. BG-EDA was prepared in DPBS and added to cells at a final concentration of 10 μg mL^{-1}. sNSP were incubated with BD-EDA for 72 h at 37 °C, 5% CO_2 in a humidified atmosphere.

2.8. Transfection of sNSP

BG-EDA/DNA complexes using model pEGFP plasmid or FXN-EGFP-expressing plasmid (FXN_M23; pPB-ef1a-FXN-IRES-eEGFP-neo) for transfection were prepared in DPBS at a w/w ratio of 20, as described for the gel electrophoresis study. For pEGFP plasmid, plasmid DNA was delivered at 0.5 or 1 μg per well. After 30 min of incubation at room temperature, 30 μL of solution

containing BG-EDA/DNA complexes was added to sNSP. After 48 h, the supernatant was removed and 200 µL of fresh medium was added. sNSP were cultured for another 48 h (4 days post-transfection) or 96 h (6 days post-transfection).

DNA transfection following delivery of pEGFP or FXN_M23 plasmid was assessed by the increase in the fluorescence intensity of EGFP expression. Transfection efficiency was expressed as the mean fluorescence intensity (MFI) in the treated cell sample normalized to the MFI of the untreated cell control.

2.9. Dissociation of sNSP for Flow Cytometry Analysis

After particle–sNSP incubation (Section 2.7) or transfection (Section 2.8), sNSP were dissociated for flow cytometry analysis. Washing and dissociation of sNSP were performed in a 96-well round-bottom plate. The cell culture medium was removed and sNSP were washed twice with 200 µL of DPBS. Additional washing was done by transferring each sNSP to a new well containing 200 µL of DPBS. The washing process—placing the sNSP in wells containing 200 µL of DPBS—was repeated twice. After the final wash, each sNSP was transferred to an empty well and 150 µL of Accutase solution was added. sNSP were allowed to dissociate for 30 min at room temperature with occasional mixing by pipetting. Next, 100 µL of 1% BSA-PBS solution was added to each well. The dissociated cells were centrifuged at 250 *g* for 7 min in the plate and the supernatant was discarded. The cell pellet was resuspended in 200 µL of 1% BSA-PBS solution and centrifuged (250 *g* for 7 min). Pelleted cells were resuspended in 200 µL of DPBS and pipetted through a cell strainer for analysis. The association of particles with the cells from the sNSP was analyzed on a BD Accuri C6 flow cytometer and is expressed as a percentage of cells that are AF_{647}-positive (for LbL Si core particles) or FITC-positive (for PS core particles). Briefly, the population of sensory neurons (excluding non-cellular fragments from digested sNSP) was

identified based on an untreated cell line control (U87 MG). The fluorescence intensity of untreated cell population was plotted as a histogram and gates were set to determine the percentage of fluorescence-positive and fluorescence-negative populations (assuming the untreated cells had no fluorescence). The gating strategy is shown in Figure S1. The same gates were applied to all other samples to enable comparison between the particles studied and to exclude from the analysis any unwashed particles that have a different scattering pattern owing to their smaller size (compared to the cell population).

2.10. Cryostat Sectioning of sNSP for Confocal Imaging

The cell culture medium was removed and sNSP were washed twice with 200 μL of DPBS. Additional washing was done by transferring each sNSP to a new well containing 200 μL of DPBS. The washing process—placing the sNSP in wells containing 200 μL of DPBS—was repeated twice. Next, sNSP were fixed with 4% paraformaldehyde for 15 min at room temperature. Paraformaldehyde was then removed and cells were washed once with 200 μL of DPBS. sNSP were kept in a 20% sucrose solution in DPBS until further processing. Before cutting into sections, sNSP were placed in OCT medium in a square cryostat mold and frozen at −20 °C. At least 20 sections (20 μm thick) were collected for each sNSP.

Slides were then washed by rinsing in DPBS until traces of the OCT medium were removed. Slides were placed in Hoechst solution (1:10000 in DPBS) and incubated for 5 min at room temperature, followed by three rinses with DPBS. For membrane staining, slides were placed in WGA-AF_{488} solution (5 μg mL^{-1}) and incubated for 5 min at room temperature, followed by three rinses with DPBS. Slides were then air-dried in the fume hood. Thin glass slides were placed on top of the samples mounted with few drops of Pro Gold anti-fade mounting media. Cells were

imaged with a Nikon A1R confocal microscope equipped with a 20× air objective or a 40× water objective.

2.11. Minimum Information Reporting in Bio–Nano Experimental Literature (MIRIBEL)

The studies conducted herein, including material characterization, biological characterization, and experimental details, conform to the MIRIBEL reporting standard for bio–nano research,[34] and we include a companion checklist of these components herein.

3. RESULTS AND DISCUSSION

3.1. Particle Preparation

Neurospheres are 3D cell models that mimic aggregates of heterogeneous sensory neurons found in the DRG within the peripheral nervous system.[29] Templated particles were selected as a well-characterized particle system with tunable physicochemical properties such as size and surface chemistry to investigate particle association with neurospheres. LbL assembly was chosen as a method of particle preparation to deposit a multilayered film on a spherical template. Templates of various sizes, materials, and densities are commercially available and can be engineered further to modify the particle properties. In the present study, two types of templates were selected, Si and PS, based on their amenability to surface modification by film deposition and their use as particle templates for biomedical applications, including cancer therapies and vaccines, as demonstrated by previous studies.[35,36] The use of particles of the same size and surface charge but of different materials enables comparison of the effect of particle density on particle interactions with sNSP. The densities of Si and PS are respectively 1.8 and 1.05 g cm^{-3}. Therefore, the particles with a Si core are expected to show a faster sedimentation rate compared with the particles with a PS core. In addition, three different sizes for each type of template were examined: 235, 387, and 837 nm for Si particles, and 288, 450, and 1000 nm for PS particles. To prepare LbL Si particles, the

template was primed with PEI to introduce a positive charge on the surface and facilitate the growth of the film through the electrostatic interaction of negatively charged PSS and positively charged PLArg. The film was formed with AF_{647}-PLArg to fluorescently label the particles and allow monitoring of the particles by flow cytometry and confocal laser scanning microscopy. To investigate the effect of particle surface charge on cell association, particles with negative and positive net surface charge were prepared, namely negatively charged particles terminated with PSS (giving the final shell structure [PEI-PSS-(AF_{647}-PLArg)-PSS]) and positively charged particles terminated with PLArg (final shell structure [PEI-PSS-(AF_{647}-PLArg)]). PS particles were obtained as FITC-labeled, eliminating the need of an additional fluorescent material in the film. For the PS template, the bare particles served as a model of a negatively charged system, whereas the PEI-coated PS particles represented a positively charged PS system. The ζ-potential of the particles, which is indicative of surface charge, was measured using microelectrophoresis. The physicochemical properties of the different particle systems examined, including size, surface charge, and composition, are summarized in Table 1 and representative imaging analysis of the particles is shown in Figure S2. To improve reproducibility, reporting, and re-analysis, this study conforms to the MIRIBEL standard,[34] and a companion checklist is provided in the Supporting Information.

Table 1. Particle characterization

Particle system	Template	Density[a] (g cm^{-3})	Size[b] (nm)	Charge[c] (mV)	Outer layer	Fluorophore
Si 837 nm (+)	Silica	1.8	832	22 ± 3	PLArg	AF647 (shell)
Si 837 nm (−)	Silica	1.8	832	-40 ± 6	PSS	AF647 (shell)
Si 387 nm (+)	Silica	1.8	387	30 ± 7	PLArg	AF647 (shell)
Si 387 nm (−)	Silica	1.8	387	-42 ± 4	PSS	AF647 (shell)
Si 235 nm (+)	Silica	1.8	235	29 ± 8	PLArg	AF647 (shell)
Si 235 nm (−)	Silica	1.8	235	-43 ± 7	PSS	AF647 (shell)
PS 1000 nm (+)	Polystyrene	1.05	1000	38 ±4	PEI	FITC (core)
PS 1000 nm (−)	Polystyrene	1.05	1000	-39 ± 4	–[d]	FITC (core)
PS 450 nm (+)	Polystyrene	1.05	450	35 ± 5	PEI	FITC (core)
PS 450 nm (−)	Polystyrene	1.05	450	-37 ± 6	–[d]	FITC (core)
PS 288 nm (+)	Polystyrene	1.05	288	19 ± 8	PEI	FITC (core)
PS 288 nm (−)	Polystyrene	1.05	288	-44 ± 8	–[d]	FITC (core)
BG-EDA (free)	Soft particle (glycogen)	N/A[e]	24 ± 4	33 ± 4	–[d]	AF647
BG-EDA (complex)	Soft particle (complexed with DNA)	N/A[e]	184 ± 11	5 ± 2	–[d]	AF647 (BG-EDA)

[a]Density is based on information from the manufacturer.

[b]Size is based on information from the manufacturer (PS and Si cores) or dynamic light scattering measurements at 25 °C (BG-EDA; BG-EDA complex).

[c]ζ-Potential was measured by electrophoresis at 25 °C. These values represent the average and standard deviation of 10 measurements.

[d]–, not applicable.

[e]N/A, not available.

3.2. Particle Association with sNSP Assessed by Flow Cytometry

hESC-Derived sNSP were used as in vitro models to assess the effect of the physicochemical properties of particles on their distribution in 3D neuronal cell models. The binding between particles of different sizes and neurons was first studied by flow cytometry to measure the association of the particles with cells in the sNSP. After incubation of fluorescently labeled particles with the sNSP, the sNSP were dissociated to obtain single cells for flow cytometry analysis. The association of the positively charged particles with cells within the sNSP decreased with increasing sizes of the Si core from 65% (Si 235 nm (+)) to 20% (Si 837 nm (+)) (Figure 1A). To understand the influence of surface charge on the association of particle with cells within the sNSP, the association of particles of different compositions in the outer layer was investigated. Particle surface charge was modulated by varying the outer layer of the particles. To confer a negative charge, PSS was deposited as the outer layer and to confer a positive charge, particles were terminated with a PLArg outer layer. Significantly higher association was observed for the 235 nm positively charged particles (PLArg-terminated) compared with the negatively charged particles (PSS-terminated) (Figure 1B). Although the 837 nm PLArg-terminated Si particles also showed slightly higher sNSP association than its negative counterpart, the difference was statistically non-significant (Figure 1B), similarly to the (statistically non-significant) difference observed for the 387 nm Si particles. Likewise, the effects of charge and size on the association of PS-based particles with sNSP were statistically non-significant. Negatively charged 288 nm PS particles appeared to show the highest association of PS-based particles with sNSP.

The association of Si and PS particles was then compared to examine the effect of particle density on the association of cells from sNSP. The particles examined had comparable size and charge, but a different core density, i.e., Si (1.8 g cm^{-3}) and PS (density 1.05 g cm^{-3}). The results

in Figure 1C and 1D indicate a generally higher association with cells from sNSP for particles with a Si core than with a PS core for a given particle size and charge. A limitation of this experiment is that although their densities differ, the diameters of the Si and PS particles are not identical (e.g., Si 235 nm and PS 288 nm). However, a previous study on immune cell interactions of polymer particles in the presence or absence (capsule) of a solid mesoporous Si template suggests that density influences cell binding of particles of the same size.[37] Hence, we would expect the denser Si-based particles to display higher binding than PS-based particles of the same size and surface properties.

The results in Figure 1 were obtained after incubation of the various particles with sNSP under static (non-mixing) conditions. To investigate any potential effect of particle sedimentation during incubation, the particles were incubated with sNSP under dynamic (orbital mixing) conditions in a parallel experiment. As indicated from Figure S3, which compares static condition data in Figure 1 with corresponding samples incubated under dynamic conditions, no significant difference in particle–sNSP association was observed when particles were incubated with sNSP with (MIX) or without (STAT) mixing.

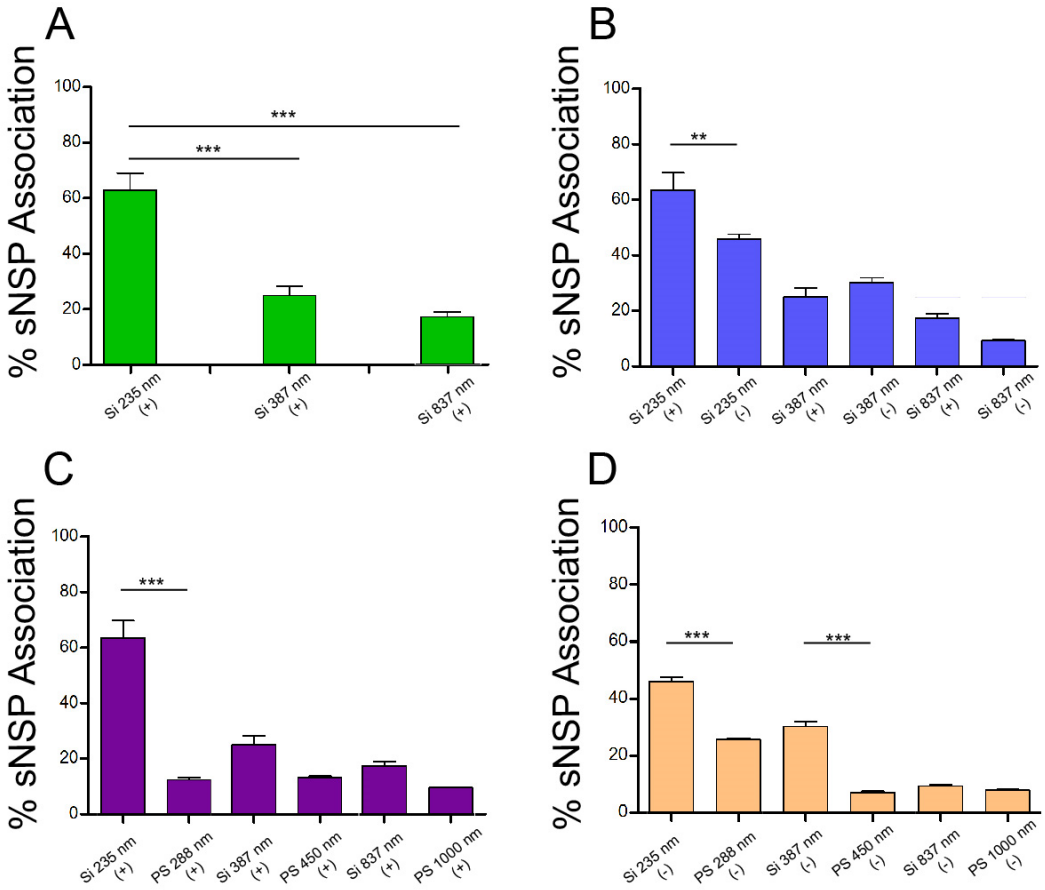

Figure 1. Association of particles with sNSP. Effect of Si particle (A) size and (B) charge on particle association with sNSP evaluated by flow cytometry. Effect of core density (PS or Si particles) on association of (C) positively and (D) negatively charged particles with sNSP. Data are shown as the average mean ± standard error of the mean (n = 4). Statistical analyses were performed using one way-ANOVA with Tukey's multiple comparison test. ***$p < 0.001$.

3.3. Particle Distribution in sNSP Assessed by Confocal Microscopy

Confocal microscopy was used to analyze the distribution of the particles in hESC-derived sNSP. Frozen sNSP were cut into 20 µm-thick sections. Representative cross-sections from the surface and center of the sphere are shown in Figure 2 (for the 235, 387, and 837 nm Si particles) and Figure 3 (for the 288, 450, and 1000 nm PS particles). Higher-resolution images of sNSP

cross-sections are shown in Figures S4–S9. Imaging of sections derived from sNSP treated with LbL Si particles largely confirmed the results obtained by flow cytometry and suggests that among the particles we examined the positively charged 235 nm are most efficient for sNSP penetration (Figure 1A, Figure 2A and 2B, Figure 4). It also indicated that although a large proportion of the particles accumulate at the sNSP periphery, the smallest particles (235 nm) can penetrate deep into the spheres (up to 250 μm from the surface) regardless of their surface charge (Figure 2A and 2B, Figure S4). Contrary to the flow cytometry results that showed low association of PS particles with sNSP (Figure 1C, D), PS particles could be observed inside sections up to ~200 μm of depth (Figure S7). Interestingly, with the large positively charged particles, i.e. 837 nm PLArg-terminated LbL Si particles and 1000 nm PEI-coated PS particles, the binding observed from flow cytometry (Figure 1C) was localized mainly on the surface of the spheres (Figures 2A and 3A). This may indicate that the particles are less able to penetrate the sNSP, which may be due to their size and hence a limited ability to cross tight cell–cell junctions within sNSP, and/or electrostatic interactions between the positively charged particles and negatively charged ECM components. Overall, the effect of charge on sNSP penetration as observed by confocal microscopy is two-fold: (i) larger negatively charged 837 nm Si- and 1000 nm PS-based particles show less binding and penetration than their positively charged counterparts, which may be caused by electrostatic repulsion between negatively charged particles and negatively charged ECM components; and (ii) smaller negatively charged 235 nm Si- and 288 nm PS-based particles are also able to penetrate the sNSP (Figures S4 and S7) similarly to their positively charged counterparts. It is possible that the porosity of the sNSP allows smaller (<288 nm) particles to penetrate more freely regardless of charge although charge can influence subsequent cell binding or internalization, which is consistent with the flow cytometry results for Si particles (Figure 1B).

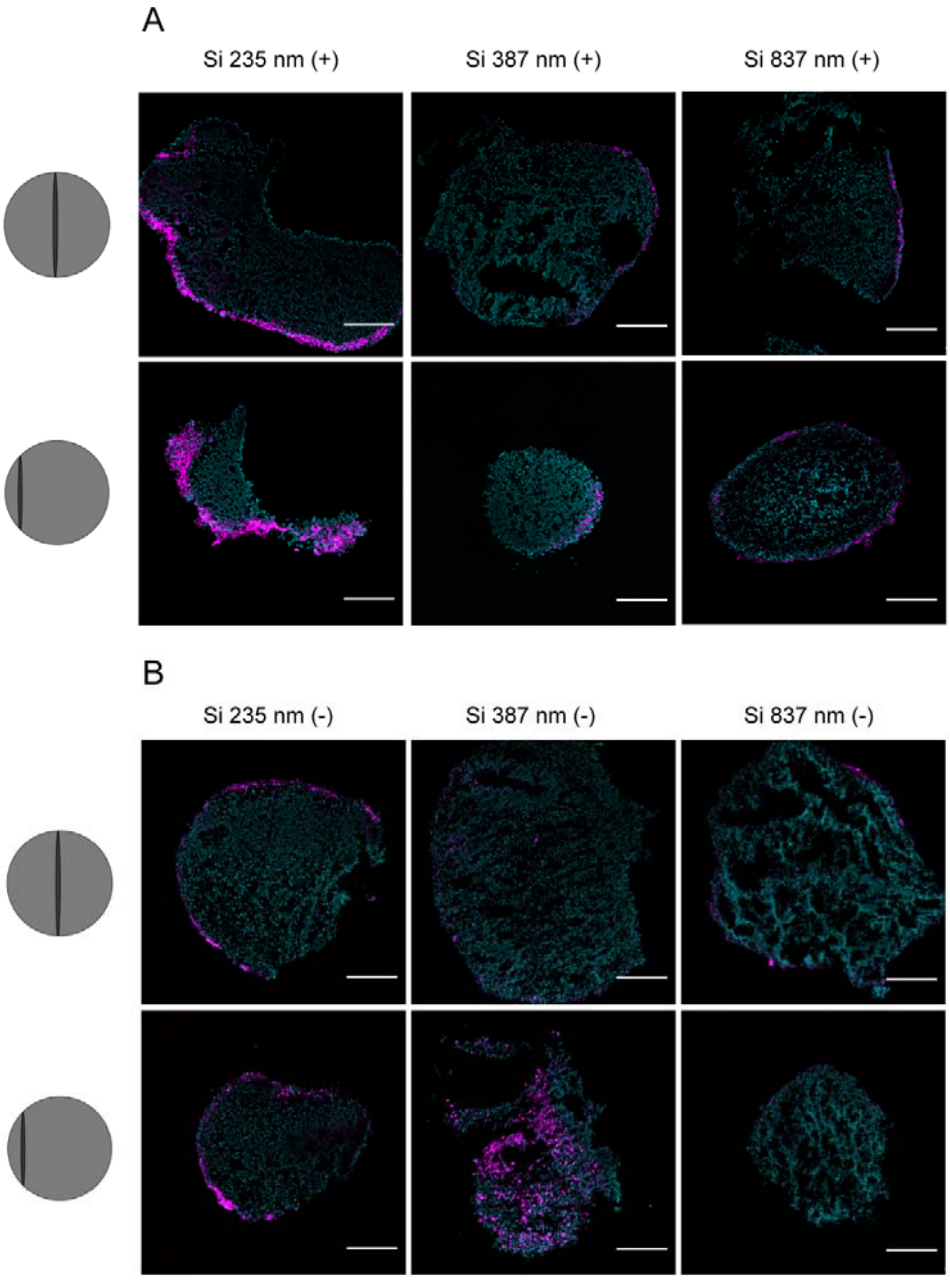

Figure 2. Distribution of LbL Si particles in sNSP. Confocal microscopy images of representative cross-sections taken from the center and surface of the sNSP after treatment with (A) positively and (B) negatively charged LbL Si particles. Particles were prepared with Si cores of 235, 387, or 837 nm. Nuclei were stained with Hoechst and pseudo-colored as cyan and AF_{647}-labeled particles are in magenta. Scale bars are 100 μm.

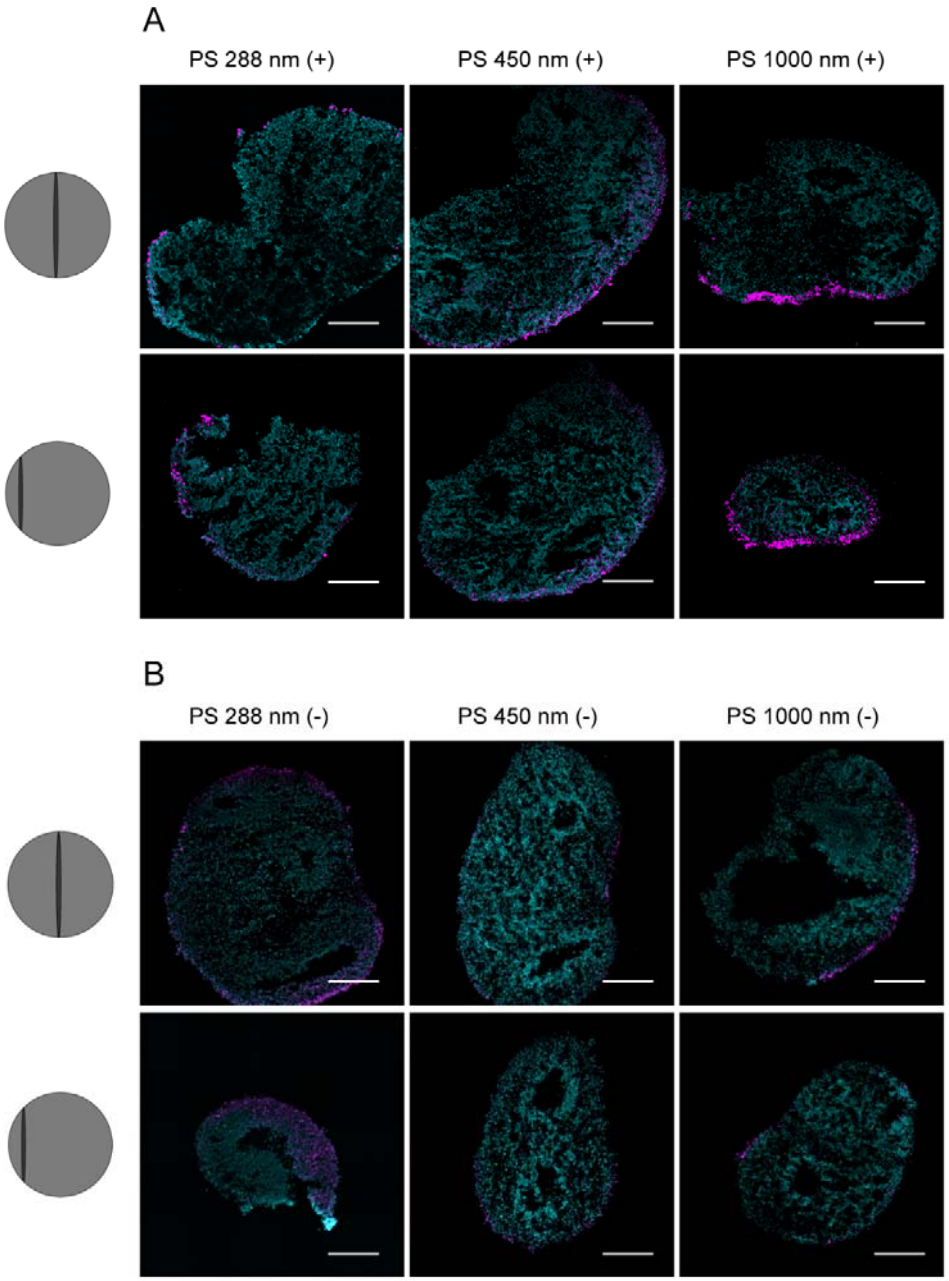

Figure 3. Distribution of PS particles in sNSP. Confocal microscopy images of two representative cross-sections taken from the center and surface of the sNSP after treatment with (A) positively and (B) negatively charged PS particles. Particles were prepared with PS cores of 288, 450, or 1000 nm. Nuclei were stained with Hoechst and pseudo-colored as cyan and FITC-labeled particles are in magenta. Scale bars are 100 μm.

To further examine the penetration of the Si particles in sNSP, the middle section of a representative sphere was imaged at different depths i.e. at the surface (<50 μm), 100–150 μm, and 200–250 μm (Figure 4). All LbL Si particles were located close to the surface of the sNSP and the 387 nm Si particles penetrated the sNSP up to a depth of 150 μm. The smallest (235 nm) particles terminated with PLArg could reach cells at depths of 250 μm. These results therefore suggest that for particles with a solid template, a small particle diameter (<288 nm) and a positive surface charge might enhance penetration inside sNSP. These findings may be useful in targeting the sensory neurons of the DRG in the peripheral nervous system, which are implicated in pain management and ataxia.[38, 39] Although nanoparticle design for targeting the human nervous system is most often discussed in the context of crossing the blood–brain barrier (BBB) for drug delivery to the brain, where nanoparticles with sizes of <100 nm are preferred,[40] targeting the sensory neurons of the DRG bypasses the BBB as administration can be performed intrathecally.

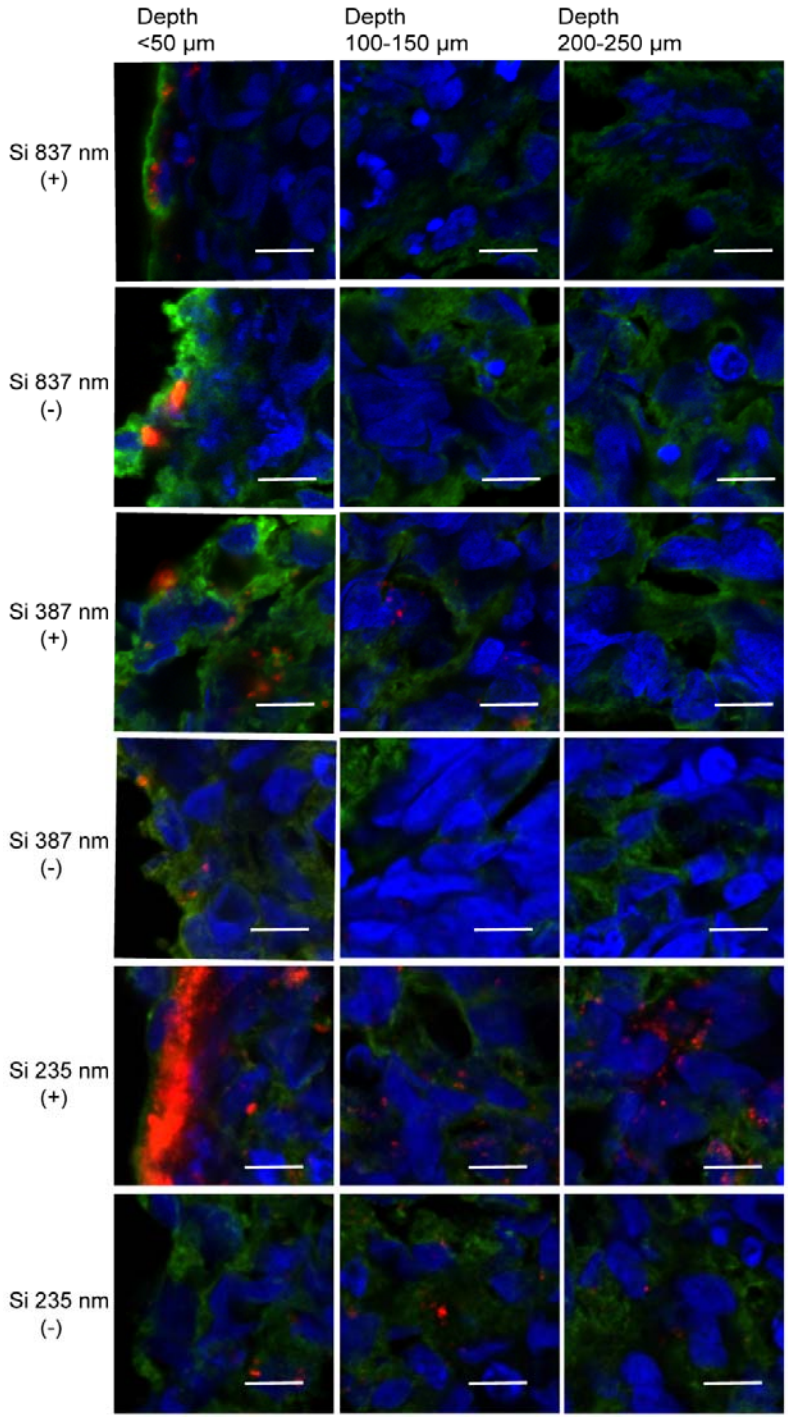

Figure 4. Penetration of LbL Si particles into sNSP. Images show the middle section of a representative sphere at different depths. Nucleus (stained with Hoechst) is blue, cell membrane (WGA-AF_{488}) is green, and AF_{647}-labeled particles are red. Scale bars are 20 µm.

3.4. Amine-Modified BG as a Delivery System of DNA to sNSP

In addition to examining solid particles with Si and PS cores, a flexible, "soft" particle system based on bovine-derived glycogen (Figure S2C) was studied. Glycogen is a naturally occurring biomolecule, structured as a nanoparticle with a diameter of ~20 nm and an inherent negative charge. The chemical modification of BG with EDA to introduce amine groups has been previously demonstrated as a strategy to enable the loading of negatively charged nucleic acid to form polyplexes.[33] BG-EDA complexed with siRNA has been found to penetrate a 3D model of prostate cancer and confer gene silencing. Other glycogen derivatives obtained by modification with 3-(dimethylamino)-1-propylamine and 1-(2-aminoethyl) piperazine have been used to form 100–250 nm complexes with DNA, which were effective for transfection of brain tissue of Sprague rats.[41]

Herein, the penetration of free BG-EDA nanoparticles into sNSP was first investigated by confocal microscopy. The presence of evenly distributed nanoparticles in the cross-sectional images of the surface and the center of the sNSP indicates deep penetration into the sNSP. Representative confocal images are presented in Figure 5.

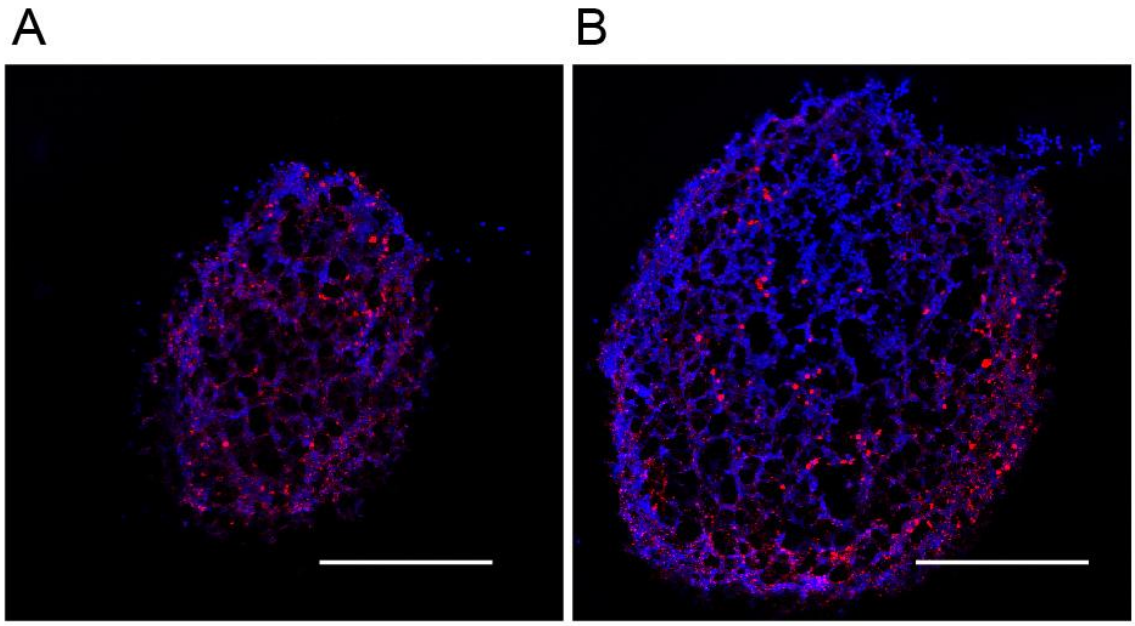

Figure 5. Distribution of BG-EDA in sNSP. Images show two representative sections from the (A) surface and (B) center of the sNSP. Nucleus (stained with Hoechst) is blue and AF_{647}-labeled BG-EDA particles are red. Scale bars are 100 μm.

The ability of BG-EDA to complex plasmid DNA and transfect cells within the sNSP was examined. Polyplex formation between BG-EDA and a model plasmid expressing green fluorescent protein (pEGFP) was studied by agarose gel electrophoresis (Figure 6A). A fixed amount of DNA (0.5 μg) was incubated with varying amounts of glycogen to obtain polyplexes with various BG-EDA/DNA weight ratios. The absence of a DNA band indicates polyplex formation, whereas the presence of a DNA band indicates the presence of excess or free DNA in the mixture. Figure 6A indicates that effective complex formation occurs within a BG-EDA/DNA ratio range of 20–30. For transfection experiments, a BG-EDA/DNA ratio of 20 was chosen, at which the polyplex had a diameter of approximately 180 nm and a slightly positive charge, as measured by dynamic light scattering (DLS) and microelectrophoresis, respectively (Table 1). AFM imaging of the BG-EDA/DNA polyplexes under aqueous conditions shows nanostructures

consistent with this size (Figure S10), as well as free plasmid and BG-EDA owing to the incomplete complexation at a 20 w/w BG-EDA/DNA ratio. For comparison, polyplexes consisting of BG-EDA and siRNA had mean diameters of 150 nm in PBS as measured by DLS.[33] When in culture media, the size of the BG-EDA/nucleic acid complexes is expected to increase slightly owing to the adsorption of serum proteins, as previously demonstrated using stochastic optical reconstruction microscopy.[42]

The association of BG-EDA/DNA polyplexes with cells from within sNSP was compared with that of free BG-EDA (Figure 6B). Both complexed and free BG-EDA showed high cell association with 60% of cells within the sNSP associating with free BG-EDA and over 80% of cells for BG-EDA/DNA.

Finally, the functional effect of pEGFP plasmid DNA transfected in sNSP (Figure 6C) was assessed. BG-EDA/pEGFP polyplexes (w/w ratio 20) were incubated with sNSP for 4 or 6 days. A 35% increase in the EGFP expression was observed 4 days post-transfection in cells treated with BG-EDA/pEGFP polyplexes (w/w ratio 20) compared to untreated cells. The expression of EGFP was confirmed by confocal microscopy (Figure 6D and Figure S11). This effect was enhanced by delivering a higher amount of plasmid (from 0.5 to 1 μg) and by increasing the incubation time from 4 to 6 days, i.e., EGFP expression was measured 6 days post-transfection. As sNSP provide a useful in vitro platform to screen drugs/compounds to treat FRDA, the delivery of a therapeutically relevant plasmid DNA encoding *pEGFP-FXN* (0.5 μg per well) was examined (Figure S12). The results are consistent with those obtained for the model plasmid, showing approximately 55% increase in EGFP protein expression in sNSP that can potentially be further modulated by engineering the promoter region of the plasmid. In addition, BG-EDA has been shown to be highly biocompatible when injected systemically in a healthy mouse model.[33]

Although a more detailed toxicological and immunological characterization of BG-EDA is warranted, our results show the potential of BG-EDA in gene therapy aimed at FRDA.

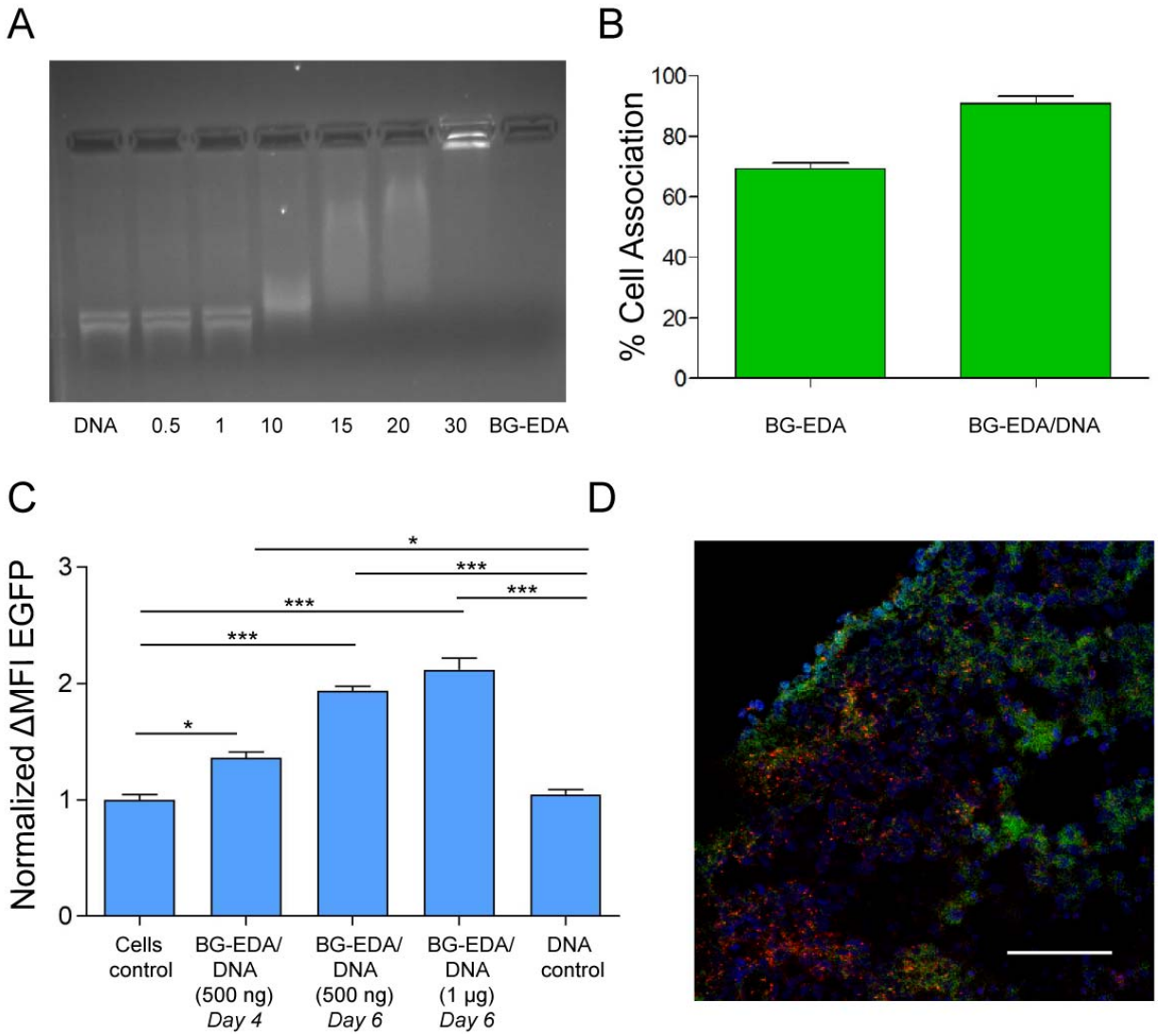

Figure 6. Characterization of BG-EDA/DNA complexes. (A) Agarose gel electrophoresis analysis of plasmid DNA complexation with BG-EDA: Lane 1, plasmid DNA; Lanes 2–7, BG-EDA/DNA complexes at different weight ratios; and Lane 8, BG-EDA control. (B) Glycogen cell association evaluated by flow cytometry, showing association of AF_{647}-labeled BG-EDA and BG-EDA/DNA complexes at w/w ratio 20 with neurospheres. (C) Glycogen-mediated DNA transfection as measured by an increase in EGFP fluorescence after treatment with BG-

EDA/pEGFP formed at w/w ratio 20. MFI was normalized against "Cells control". Data are shown as the average mean ± standard error of the mean ($n = 3$). Statistical analyses were performed using one way-ANOVA with Tukey's multiple comparison test. ***$p < 0.001$. (D) Confocal microscopy image of a section of sNSP transfected with AF_{647}-labeled BG-EDA complexed with pEGFP. Scale bar is 100 μm.

4. CONCLUSIONS

In the present study, the effects of particle size, surface charge, and density on the distribution and penetration of different particle systems in 3D human sensory neuronal models were investigated. Particles with "solid" silica or polystyrene cores were prepared via LbL film deposition or adsorption on spherical templates, respectively. The results show that a positive surface charge and a size within 230–280 nm facilitate penetration of the particles to the interior of sNSP. Particles that are more dense, due to the presence of a silica core, showed enhanced penetration (up to 250 μm deep in the sphere), whereas lighter particles (PS core) with similar size and charge could penetrate the sNSP, however, less efficiently. "Soft" glycogen nanoparticles (30 nm) showed an even distribution within the sNSP. When assembled with plasmid DNA to form a polyplex (180 nm), the polyplexes efficiently penetrated sNSP and importantly, the delivered pEGFP plasmid DNA was functional as demonstrated by the expression of EGFP in neurons up to 6 days post-transfection. This work provides guidance on particle design for delivery to 3D neuronal culture. Although nanoparticle design for crossing the blood–brain barrier has been a major focus in brain delivery research, other routes for brain delivery and in combination with cell replacement therapy can be potentially exploited to tackle some of the currently incurable neurodegenerative diseases including FRDA. We demonstrate that the stem cell-derived 3D neuronal cell model used in this work is a useful platform to screen various particle formulations

and could be used in future studies to identify effective nanomedicines for drug delivery to neurons.

ASSOCIATED CONTENT

Supporting Information. Confocal microscopy images of coated Si and PS particles; atomic force microscopy image of BD-EDA nanoparticles; flow cytometry data showing the comparison of static versus dynamic incubation conditions; gray scale confocal images of sNSP cross-sections after incubation with positively charged and negatively charged Si and PS particles of various sizes; transfection of sNSP with BD-EDA/DNA and BG-EDA particles; normalized MFI of EGFP expression 4 days post-transfection of sNSP with frataxin-EGFP-expressing plasmid (FXN_M23); MIRIBEL checklist including material characterization, biological characterization and experimental details.

AUTHOR INFORMATION

Corresponding Author

Christina Cortez-Jugo – E-mail address: christina.cortez@unimelb.edu.au
Mirella Dottori – E-mail address: mdottori@uow.edu.au
Frank Caruso – E-mail address: fcaruso@unimelb.edu.au

ACKNOWLEDGMENTS

This research was conducted and funded by the Australian Research Council Centre of Excellence in Convergent Bio-Nano Science and Technology (project number CE140100036). F.C. acknowledges the award of a National Health and Medical Research Council Senior Principal Research Fellowship (GNT1135806). S.V. was funded by a Melbourne International Research Scholarship and a Melbourne International Fee Remission Scholarship (The University of

Melbourne). This work was performed in part at the Materials Characterisation and Fabrication Platform (MCFP) at The University of Melbourne and the Victorian Node of the Australian National Fabrication Facility (ANFF) and Melbourne Histology Platform. This study was also supported by funding from the National Ataxia Foundation, Friedreich's Ataxia Research Alliance (USA), Friedreich's Ataxia Research Association Australasia, The University of Melbourne, and University of Wollongong. The experiments with hESC were performed in accordance with the Guidelines of the National Health and Medical Research Council and approved by The University of Melbourne and University of Wollongong Human Ethics Committees (#1545384 and #2017/375).

REFERENCES

1. Naldini, L. Gene Therapy Returns to Centre Stage. *Nature* **2015**, *526*, 351–360.
2. Morachis, J. M; Mahmoud, E. A.; Almutairi, A. Physical and Chemical Strategies for Therapeutic Delivery by Using Polymeric Nanoparticles. *Pharmacol. Rev.* **2012**, *64*, 505–519.
3. Chowdhury, A.; Kunjiappan, S.; Panneerselvam, T.; Somasundaram, B.; Bhattacharjee, C. Nanotechnology and Nanocarrier-Based Approaches on Treatment of Degenerative Diseases. *Int. Nano Lett.* **2017**, ***7***, 91–122.
4. Senapati, S.; Mahanta, A. K.; Kumar, S.; Maiti, P. Controlled Drug Delivery Vehicles for Cancer Treatment and Their Performance. *Signal Transduction Targeted Ther.* **2018**, *3*, 7.
5. Blanco, E.; Shen, H.; Ferrari. Principles of Nanoparticle Design for Overcoming Biological Barriers to Drug Delivery. *Nat. Biotechnol.* **2015**, *33*, 941–951.
6. Yu, B.; Tai, H. C.; Xue, W.; Lee, L. J.; Lee, R. J. Receptor-Targeted Nanocarriers for Therapeutic Delivery to Cancer. *Mol. Membr. Biol.* **2010**, *27*, 286–298.
7. Nel, A. E.; Madler, L.; Velegol, D.; Xia, T.; Hoek, E. M.; Somasundaran, P.; Klaessig, F.; Castranova, V.; Thompson, M. Understanding Biophysicochemical Interactions at the Nano–Bio Interface. *Nat. Mater.* **2009**, *8*, 543–557.

8. Wurster, E. C.; Liebl, R.; Michaelis, S.; Robelek, R.; Wastl, D. S.; Giessibl, F. J.; Goepferich, A.; Breunig, M. Oligolayer-Coated Nanoparticles: Impact of Surface Topography at the Nanobio Interface. *ACS Appl. Mater. Interfaces*, **2015**, *7*, 7891–7900.
9. Petros, R. A.; DeSimone, J. M. Strategies in the Design of Nanoparticles for Therapeutic Applications. *Nat. Rev. Drug Discovery* **2010**, *9*, 615–627.
10. Edmondson, R.; Broglie, J. J.; Adcock, A. F.; Yang, L. Three-Dimensional Cell Culture Systems and Their Applications in Drug Discovery and Cell-Based Biosensors. *Assay Drug Dev. Technol.* **2014**, *12*, 207–218.
11. Jorfi, M.; D'Avanzo, C.; Kim, D. Y.; Irimia, D. Three-Dimensional Models of the Human Brain Development and Diseases. *Adv. Healthcare Mater.* **2018**, *7*, 1700723.
12. Zanoni, M.; Piccinini, F.; Arienti, C.; Zamagni, A.; Santi, S.; Polico, R.; Bevilacqua, A.; Tesei, A. 3D Tumor Spheroid Models for In Vitro Therapeutic Screening: A Systematic Approach to Enhance the Biological Relevance of Data Obtained. *Sci. Rep.* **2016**, *6*, 19103.
13. Langhans, S. A. Three-Dimensional In Vitro Cell Culture Models in Drug Discovery and Drug Repositioning. *Front. Pharmacol.* **2018**, *9*, 6.
14. Manfredonia, C.; Muraro, M. G.; Hirt, C.; Mele, V.; Governa, V.; Papadimitropoulos, A.; Däster, S.; Soysal, S. D.; Droeser, R. A.; Mechera, R.; Oertli, D.; Rosso, R.; Bolli, M.; Zettl, A.; Terracciano, L. M.; Spagnoli, G. C.; Martin, I.; Iezzi, G. Maintenance of Primary Human Colorectal Cancer Microenvironment Using a Perfusion Bioreactor-Based 3D Culture System. *Adv. Biosyst.* **2019**, *3*, 1800300.
15. Jang, H. L.; Zhang, Y. S.; Khademhosseini, A. Boosting Clinical Translation of Nanomedicine. *Nanomedicne* **2016**, *11*, 1495–1497.
16. Centeno, E. G. Z.; Cimarosti, H.; Bithell, A. 2D Versus 3D Human Induced Pluripotent Stem Cell-Derived Cultures for Neurodegenerative Disease Modelling. *Mol. Neurodegener.* **2018**, *13*, 27.
17. Penney, J.; Ralvenius, W. T.; Tsai, L. H. Modeling Alzheimer's Disease with iPSC-Derived Brain Cells. *Mol. Psychiatry* **2020**, *25*, 148–167.
18. Chen, I. Y.; Matsa, E.; Wu, J. C. Induced Pluripotent Stem Cells: At the Heart of Cardiovascular Precision Medicine. *Nat. Rev. Cardiol.* **2016**, *13*, 333–349.

19. Cota-Coronado, A.; Ramirez-Rodriguez, P. B.; Padilla-Camberos, E.; Diaz, E. F.; Flores-Fernandez, J. M.; Avila-Gonzalez, D.; Diaz-Martinez, N. E. Implications of Human Induced Pluripotent Stem Cells in Metabolic Disorders: From Drug Discovery toward Precision Medicine. *Drug Discovery Today* **2019**, *24*, 334–341.
20. Tang-Schomer, M. D.; White, J. D.; Tien, L. W.; Schmitt, L. I.; Valentin, T. M.; Graziano, D. J.; Hopkins, A. M.; Omenetto, F. G.; Haydon, P. G.; Kaplan, D. L. Bioengineered Functional Brain-Like Cortical Tissue. *Proc. Natl. Acad. Sci. U.S.A.* **2014**, *111*, 13811–13816.
21. Chambers, S. M.; Qi, Y.; Mica, Y.; Lee, G.; Zhang, X. J.; Niu, L.; Bilsland, J.; Cao, L.; Stevens, E.; Whiting, P.; Shi, S. H.; Studer, L. Combined Small Molecule Inhibition Accelerates Developmental Timing and Converts Human Pluripotent Stem Cells into Nociceptors. *Nat. Biotechnol.* **2012**, *30*, 715–720.
22. Neely, M. D.; Litt, M. J.; Tidball, A. M.; Li, G. G.; Aboud, A. A.; Hopkins, C. R.; Chamberlin, R.; Hong, C. C.; Ess, K. C.; Bowman, A. B. DMH1, a Highly Selective Small Molecule BMP Inhibitor Promotes Neurogenesis of hiPSCs: Comparison of PAX6 and SOX1 Expression during Neural Induction. *ACS Chem. Neurosci*. **2012**, *3*, 482–491.
23. Li, W.; Sun, W.; Zhang, Y.; Wei, W.; Ambasudhan, R.; Xia, P.; Talantova, M.; Lin, T.; Kim, J.; Wang, X.; Kim, W. R.; Lipton, S. A.; Zhang, K.; Ding, S. Rapid Induction and Long-Term Self-Renewal of Primitive Neural Precursors from Human Embryonic Stem Cells by Small Molecule Inhibitors. *Proc. Natl. Acad. Sci. U.S.A.* **2011**, *108*, 8299–8304.
24. Hopkins, A. M.; DeSimone, E.; Chwalek, K.; Kaplan, D. L. 3D In Vitro Modeling of the Central Nervous System. *Prog. Neurobiol.* **2015**, *125*, 1–25.
25. Talib, S.; Shepard, K. A. Unleashing the Cure: Overcoming Persistent Obstacles in the Translation and Expanded Use of Hematopoietic Stem Cell-Based Therapies. *Stem Cells Transl. Med.* **2020**, *9*, 420–426.
26. Piguet, F.; de Montigny, C.; Vaucamps, N.; Reutenauer, L.; Eisenmann, A.; Puccio, H. Rapid and Complete Reversal of Sensory Ataxia by Gene Therapy in a Novel Model of Friedreich Ataxia. *Mol. Ther.* **2018**, *26*, 1940–1952.
27. Crombie, D. E.; Curl, C. L.; Raaijmakers, A. J. A.; Sivakumaran, P.; Kulkarni, T.; Wong, R. C. B.; Minami, I.; Evans-Galea, M. V.; Lim, S. Y.; Delbridge, L.; Corben, L. A.; Dottori, M.; Nakatsuji, N.; Trounce, I. A.; Hewitt, A. W.; Delatycki, M. B.; Pera, M. F.;

Pebay, A. Friedreich's Ataxia Induced Pluripotent Stem Cell-Derived Cardiomyocytes Display Electrophysiological Abnormalities and Calcium Handling Deficiency. *Aging* **2011**, *9*, 1440–1449.

28. Abu-Bonsrah, K. D.; Viventi, S.; Newgreen, D. F; Dottori, M. Generation of Neural Crest Progenitors from Human Pluripotent Stem Cells. *Methods Mol. Biol.* **2019**, *1976*, 37–47.
29. Alshawaf, A. J.; Viventi, S.; Qiu, W.; D'Abaco, G.; Nayagam, B.; Erlichster, M.; Chana, G.; Everall, I.; Ivanusic, J.; Skafidas, E.; Dottori, M. Phenotypic and Functional Characterization of Peripheral Sensory Neurons Derived from Human Embryonic Stem Cells. *Sci. Rep.* **2018**, *8*, 603.
30. Zeng, Y.; Kurokawa, Y.; Zeng, Q.; Win-Shwe, T. T.; Nansai, H.; Zhang, Z.; Sone, H. Effects of Polyamidoamine Dendrimers on a 3-D Neurosphere System Using Human Neural Progenitor Cells. *Toxicol. Sci.* **2016**, *152*, 128–144.
31. Hoelting, L.; Scheinhardt, B.; Bondarenko, O.; Schildknecht, S.; Kapitza, M.; Tanavde, V.; Tan, B.; Lee, Q. Y.; Mecking, S.; Leist, M.; Kadereit, S. A 3-Dimensional Human Embryonic Stem Cell (hESC)-Derived Model to Detect Developmental Neurotoxicity of Nanoparticles. *Arch. Toxicol.* **2013**, *87*, 721–733.
32. Leite, P. E. C.; Pereira, M. R.; Harris, G.; Pamies, D.; Dos Santos, L. M. G.; Granjeiro, J. M.; Hogberg, H. T.; Hartung, T.; Smirnova, L. Suitability of 3D Human Brain Spheroid Models to Distinguish Toxic Effects of Gold and Poly-lactic Acid Nanoparticles to Assess Biocompatibility for Brain Drug Delivery. *Part. Fibre Toxicol.* **2019**, *16*, 22.
33. Wojnilowicz, M.; Besford, Q. A.; Wu, Y. L.; Loh, X. J.; Braunger, J. A.; Glab, A.; Cortez-Jugo, C.; Caruso, F.; Cavalieri, F. Glycogen-Nucleic Acid Constructs for Gene Silencing in Multicellular Tumor Spheroids. *Biomaterials* **2018**, *176*, 34–49.
34. Faria, M.; Bjornmalm, M.; Thurecht, K. J.; Kent, S. J.; Parton, R. G.; Kavallaris, M.; Johnston, A. P. R.; Gooding, J. J.; Corrie, S. R.; Boyd B. J.; Thordarson, P.; Whittaker, A. K.; Stevens, M. M.; Prestidge, C. A.; Porter, C. J. H.; Parak, W. J.; David, T. P.; Crampin, E. J.; Caruso, F. Minimum Information Reporting in Bio–Nano Experimental Literature. *Nat. Nanotechnol.* 2018, **13**, 777–785.
35. Poon, Z.; Chang, D.; Zhao, X.; Hammond, P. T. Layer-by-Layer Nanoparticles with a pH-Sheddable Layer for In Vivo Targeting of Tumor Hypoxia. *ACS Nano* **2011**, *5*, 4284–4292.

36. Gause, K. T.; Yan, Y.; Cui, J.; O'Brien-Simpson, N. M.; Lenzo, J. C.; Reynolds, E. C.; Caruso, F. Physicochemical and Immunological Assessment of Engineered Pure Protein Particles with Different Redox States. *ACS Nano* **2015**, *9*, 2433–2444.
37. Cui, J.; De Rose, R.; Alt, K.; Alcantara, S.; Paterson, B. M.; Liang, K.; Hu, M.; Richardson, J. J.; Yan, Y.; Jeffery, C. M.; Price, R. I.; Peter, K.; Hagemeyer, C. E.; Donnelly, P. S.; Kent, S. J.; Caruso, F. Engineering Poly(ethylene glycol) Particles for Improved Biodistribution. *ACS Nano*, **2015**, *9*, 1571–1580.
38. Dubin, A. E.; Patapoutian, A. Nociceptors: The Sensors of the Pain Pathway. *J. Clin. Invest.* **2010**, *120*, 3760–3772.
39. Griso, O.; Puccio, H. Primary Cultures of Pure Embryonic Dorsal Root Ganglia Sensory Neurons as a New Cellular Model for Friedreich's Ataxia. *Methods Mol. Biol.* **2020**, *2056*, 241–253.
40. Furtado, D.; Bjornmalm, M.; Ayton, S.; Bush, A. I.; Kempe, K.; Caruso, F. Overcoming the Blood–Brain Barrier: The Role of Nanomaterials in Treating Neurological Diseases. *Adv. Mater*. **2018**, *30*, 1801362.
41. Liang, X.; Ren, X.; Liu, Z.; Liu, Y.; Wang, J.; Wang, J.; Zhang, L. M.; Deng, D. Y.; Quan, D.; Yang, L. An Efficient Nonviral Gene-Delivery Vector Based on Hyperbranched Cationic Glycogen Derivatives. *Int. J. Nanomedicine* **2014**, *9*, 419–435.
42. Wojnilowicz, M.; Glab, A.; Bertucci, A.; Caruso, F.; Cavalieri, F. Super-Resolution Imaging of Proton Sponge-Triggered Rupture of Endosomes and Cytosolic Release of Small Interfering RNA. *ACS Nano* **2019**, *13*, 187–202.

Table of Content graphic

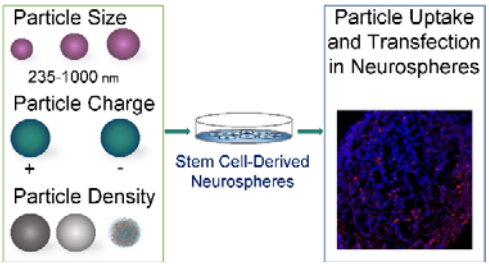

Author/s:
Czuba-Wojnilowicz, E; Miellet, S; Glab, A; Viventi, S; Cavalieri, F; Cortez-Jugo, C; Dottori, M; Caruso, F

Title:
Distribution of Particles in Human Stem Cell-Derived 3D Neuronal Cell Models: Effect of Particle Size, Charge, and Density

Date:
2020-08-01

Citation:
Czuba-Wojnilowicz, E., Miellet, S., Glab, A., Viventi, S., Cavalieri, F., Cortez-Jugo, C., Dottori, M. & Caruso, F. (2020). Distribution of Particles in Human Stem Cell-Derived 3D Neuronal Cell Models: Effect of Particle Size, Charge, and Density. BIOMACROMOLECULES, 21 (8), pp.3186-3196. https://doi.org/10.1021/acs.biomac.0c00626.